## Title

Composition of modern sand from the Sierra Nevada, California, USA: Implications for actualistic petrofacies of continental-margin magmatic arcs



## Journal

Journal of Sedimentary Research, 77

## ISSN

1527-1404

## Authors

Ingersoll, Raymond V.
Eastmond, Daniel J.

## Publication Date

2007-09-01

## DOI

10.2110/jsr.2007.071

Peer reviewed

Journal of Sedimentary Research

Journal of Sedimentary Research, 2007, v. 77, 784–796
Research Article
DOI: 10.2110/jsr.2007.071

# COMPOSITION OF MODERN SAND FROM THE SIERRA NEVADA, CALIFORNIA, U.S.A.: IMPLICATIONS FOR ACTUALISTIC PETROFACIES OF CONTINENTAL-MARGIN MAGMATIC ARCS

RAYMOND V. INGERSOLL AND DANIEL J. EASTMOND
*Department of Earth and Space Sciences, University of California, Los Angeles, California 90095-1567, U.S.A.*
*e-mail: ringer@ess.ucla.edu*

ABSTRACT: **The Sierra Nevada of California represents the roots of a long-lived magmatic arc (primarily Cretaceous) that is presently being dissected as the range is uplifted, beginning in the south and progressing northward. This dissection is occurring concurrently with northward migration of the Mendocino triple junction, south of which magmatic-arc activity is absent, and north of which magmatic-arc activity continues. A north-to-south transect along the Sierra Nevada represents transitions of active magmatic arc to transitional arc to dissected arc, and in the southern Sierra Nevada, to uplifted basement. Thus, analysis of composition of modern sand derived from these separate parts of the Sierra Nevada provides a test for actualistic sand(stone) petrofacies of magmatic arcs at all stages of dissection.**

**Rigorous statistical analysis of the composition of modern sand from the Sierra Nevada characterizes stages of magmatic-arc dissection. Discriminant analysis of point-count data from Sierra Nevada modern sand defines four compositional groups and distinguishes clearly between undissected-arc and uplifted-basement end members. Two intermediate compositional groups reflect the complex geologic history of the Sierra Nevada. Volcanic and plutonic rocks dominate one intermediate group; metamorphic and plutonic rocks dominate the other. The former group exhibits characteristics of Dickinson's (1985) "transitional arc," whereas the latter is equivalent to "dissected arc." No single compositional parameter is diagnostic of the degree of magmatic-arc dissection, although volcanic-lithic content clearly differentiates between "undissected" and "basement" groups. Regional compositional trends are evident when recalculated point-count data are plotted against latitude.**

**Sand composition in the southern Sierra Nevada reflects significant Cenozoic uplift of the batholith, resulting from Basin and Range extension. High concentrations of quartz and feldspar, and extreme lithic depletion are typical at the southernmost Sierra Nevada; this extreme depletion characterizes "basement uplift."**

**The primary drainage divide of the Sierra Nevada forms a rough compositional boundary between eastern and western groups. Potassium-feldspar content best distinguishes these groups, with higher values in the east.**

**Rigorous confidence regions in ternary diagrams yield results that are similar, but not identical, to hexagonal fields of compositional variation. Arithmetic means, associated with hexagonal fields, are not identical to geometric means, associated with logratio confidence regions. Definition of sand(stone) provenance groups, in general, depends on both data-acquisition methods (e.g., Gazzi–Dickinson method) and statistical methods (e.g., Weltje method), so that direct comparison of data analyzed using different methods is unwarranted.**

## INTRODUCTION

Sand(stone) composition, a useful indicator of modern and ancient tectonic environment, provides important constraints on the evolution of Cordilleran magmatic arcs in western North America and other convergent margins (e.g., Dickinson and Rich 1972; Ingersoll 1978, 1983; Dickinson 1985). Dissection of one of the major arcs of the Cordillera is observed in the Sierra Nevada of eastern California (Fig. 1). Northward migration of the Mendocino triple junction is reflected in northward retreat of active volcanism to Mount Lassen and the Cascade Range, and in exposure of the Sierra Nevada batholith during the late Cenozoic (Dickinson and Snyder 1979; Atwater and Stock 1998; Dickinson 2002). Thus, a north–south transect of the Sierra Nevada can be used as a proxy for arc dissection through time (Eastmond and Ingersoll 2003; Eastmond 2004; Ingersoll and Eastmond 2004).

The purpose of this study is twofold. Analysis of Sierra Nevada sand composition is a direct test of models for sand(stone) composition of magmatic arcs and their dissection through time (e.g., Dickinson and Rich 1972; Ingersoll 1978, 1983; Dickinson 1985). Secondly, previous studies of active-margin sand(stone) composition have relied entirely on summary statistics (e.g., Ingersoll 1978, 1983; Dickinson 1985; Kretchmer 1987; Marsaglia and Ingersoll 1992; Ingersoll et al. 1993), whereas this study compares summary statistics with alternative methods facilitated by new software for the purpose of rigorous compositional analysis (i.e., Weltje 2002, 2004).

## REGIONAL GEOLOGY AND TECTONIC HISTORY

The Sierra Nevada represents a 600-km-long segment of the Cordilleran arc of North America. The Sierra Nevada arc, presently inactive along most of its length, is the product of multiple phases of Mesozoic–Cenozoic magmatism, tectonic uplift, and accretion of exotic terranes (e.g., Schweickert 1981; Cowan and Bruhn 1992; Miller et al. 1992; Saleeby and Busby-Spera 1992; Ingersoll 1997; and references

 1527-1404/07/077-784/$03.00

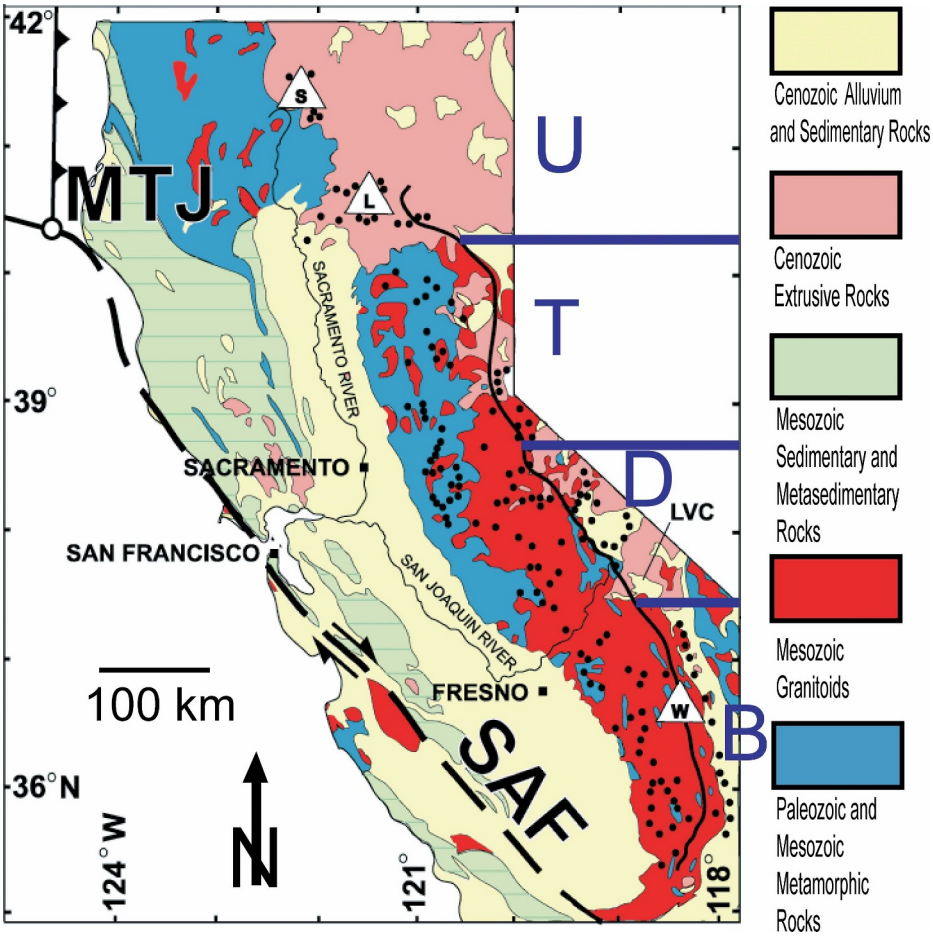


FIG. 1.—Map of northern and central California, showing specimen locations (black dots, $n = 156$), major geologic features (dashed line = San Andreas fault [SAF], open circle = Mendocino triple junction [MTJ]), and selected physical features (S = Mt. Shasta, L = Mt. Lassen, W = Mt. Whitney, LVC = Long Valley caldera). Cascadia subduction zone is shown as serrated line, with teeth on upper plate. The primary drainage divide of the Sierra Nevada is indicated by the heavy curvilinear solid line. Heavy blue lines represent approximate latitudinal boundaries separating U (undissected arc), T (transitional arc), D (dissected arc) and B (basement uplift).

therein). The following brief summary of the paleotectonic history of the Sierra Nevada utilizes models preferred by Ingersoll (1997); alternative models are discussed in the above references.

Following Neoproterozoic breakup of the supercontinent Rodinia, tectonic quiescence persisted through much of the early Paleozoic at the site of the future Sierra Nevada (Poole et al. 1992; Ingersoll 1997; and references therein). The western margin of North America maintained an intraplate setting until a proforeland (peripheral foreland) basin formed at the onset of the Antler orogeny in the Late Devonian (Speed and Sleep 1982; Burchfiel et al. 1992). The intraplate margin was dragged into a west-dipping subduction zone, opposite that of the modern Cascadia arc (Fig. 1). Contact between the continent and the island arc created the Antler orogen, temporarily ending subduction. A transform margin may have developed following the Antler orogeny, although relations are ambiguous (Ingersoll 1997; Dickinson and Lawton 2003).

The Permian–Triassic Sonoma orogeny also likely involved a west-dipping subduction zone. The collision of North America with the microcontinent Sonomia accreted continental crust to the Cordilleran margin and led to a reversal in subduction polarity (Speed 1979; Burchfiel et al. 1992; Ingersoll 1997). This polarity reversal initiated continental-arc magmatism along the Cordilleran margin (Busby-Spera 1988). Remnants of the Late Triassic batholith are exposed only along the eastern edge of the central Sierra Nevada (Schweickert 1976; Stern et al. 1981).

In the Late Jurassic, another west-dipping subduction zone and island arc approached the continent-margin arc. The oceanic plate between the two arcs sank into the mantle as the ocean basin closed (Schweickert and Cowan 1975; Ingersoll 1997). Accretion of the island arc and obduction of young, buoyant ophiolite complexes constituted the Nevadan orogeny (162–150 Ma) (Schweickert 1981; Godfrey and Klemperer 1998; Ingersoll 2000). Magmatism in both arcs was overprinted by magmatism of a new east-dipping subduction zone formed in the weak backarc of the accreted terranes (Schweickert and Cowan 1975; Ingersoll 1997, 2000).

Post-Nevadan magmatic activity generated most of the presently exposed Sierra Nevada batholith (120–80 Ma) (Hamilton 1978; Chen and Moore 1982; Bateman 1992); concurrently, the Great Valley forearc basin filled with mainly volcanogenic detritus (Dickinson and Rich 1972; Ingersoll 1983; Linn et al. 1992). Granitoids dating from this period comprise most of the exposed rocks of Yosemite Valley and elsewhere in the southern Sierra Nevada (Evernden and Kistler 1970; Stern et al. 1981; Saleeby et al. 1987; Coleman and Glazner 1997). After crystallization at depths ranging from $\sim$ 3 to $>$ 23 km, the Cretaceous batholith averaged about 30–35 km in thickness prior to Cenozoic erosion (Ague and Brimhall 1988). The Cretaceous arc generated a minimum granitoid volume of $\sim$ 400,000 km$^3$ (Tobisch et al. 1995).

Throughout the Cretaceous, the magmatic front migrated steadily eastward at an average rate of $\sim$ 2.7 mm/yr (Keith 1978, 1982; Ingersoll 1979; Stern et al. 1981; Chen and Moore 1982; Ague and Brimhall 1988; Linn et al. 1992). At this time, the arc may have accommodated transpressional strain partitioning as a zone of lithospheric weakness (Busby-Spera and Saleeby 1990; Tobisch et al. 1995; Tikoff and de Saint Blanquat 1997). Eastward migration of the magmatic front quickened at the end of the Cretaceous with decreasing dip of the subducted slab and onset of the Laramide orogeny (Coney and Reynolds 1977; Keith 1978). Magmatism in the Sierra Nevada ceased abruptly at $\sim$ 80 Ma (Chen and Moore 1982).

Rapid, flat-slab subduction refrigerated the western Cordillera and produced magmatic quiescence in the Sierra Nevada (Dickinson and Snyder 1978; Bird 1988; Dumitru et al. 1991; Ward 1991). Erosion and drainage integration increased across the arc (Dickinson et al. 1979) and uplift of the batholith, from depths of several kilometers, accelerated its incision (Dickinson and Rich 1972; Ingersoll 1978; Unruh 1991; Wakabayashi and Sawyer 2001). Deeply incised rivers transported sediment across the batholithic belt, with possible eastern headwaters in the Nevadaplano (DeCelles 2004; Mulch et al. 2006). By the early Eocene, the initial phase of uplift had ended, and the batholith had been severely eroded (Unruh 1991).

In the late Eocene, the rate of convergence between the North American and Farallon (Kula?) plates suddenly decreased (Keith 1982; Bird 1988; Ward 1991). Silicic magmatism developed across the southwestern United States as the asthenosphere decompressed during slab rollback, and arc magmatism was reestablished in the Sierra Nevada by the middle Miocene (Coney and Reynolds 1977; Keith 1978; Christiansen and Yeats 1992; Ingersoll 1997; Dickinson 2002). The Sierra Nevada region may have been at low elevation, with a blanket of volcanic and volcaniclastic strata.

Initial interaction between the North American and Pacific plates at $\sim$ 29 Ma created the Mendocino triple junction (Fig. 1) (Atwater and Stock 1998). As the triple junction migrated northwest (e.g., Dickinson and Snyder 1979; Ingersoll 1982; Dickinson 2002), magmatism progressively ceased and the batholith again was exposed, as uplift proceeded from south to north. Isolated volcanism in the Coast Ranges and at Long Valley caldera (Fig. 1) was coeval with northward-retreating arc volcanism in the Sierra Nevada during the Neogene (Dickinson 1997). Arc magmatism remains active only in the Cascade arc, from Mount Lassen northward (Kretchmer 1987; Dickinson 2002) (Fig. 1). Thus, from north to south, the modern and Cenozoic volcanic arc is increasingly dissected to reveal greater erosion depths in the Mesozoic plutonic arc and associated Paleozoic–Mesozoic metamorphic rocks.

Post-Miocene uplift has been accommodated by the eastern frontal normal-fault system along the eastern edge of the Sierra Nevada. These faults are associated with Basin and Range extension (e.g., Zoback 1989; Dickinson 2002) and with continued dissection of the arc (Unruh 1991; Wakabayashi and Sawyer 2001; Jones et al. 2004). Dip slip along these faults and, to some extent, the vertical component of slip along related strike-slip faults (Wesnousky and Jones 1994; Lee et al. 2001) have generated much of the present relief in the eastern Sierra Nevada (e.g., Christensen 1966; Huber 1981; Loomis and Burbank 1988).

The relatively rigid Sierra Nevada block has been described as an incipient microplate (e.g., Dickinson 2002), which has tilted $\sim 3^\circ$ to the west (Chase and Wallace 1986; Unruh 1991). With respect to post-Miocene uplift, the effects of vertical-axis rotation of the Sierra Nevada block (e.g., Atwater and Stock 1998; Dixon et al. 2000) and of non-rigid behavior within the block (Christensen 1966; Huber 1981; Dixon et al. 2000; Wakabayashi and Sawyer 2001) are locally significant. The general tilt of the Sierra Nevada may be caused, in part, by the isostatic effect of glacial and fluvial erosion in the High Sierra and sediment loading in the Great Valley (Chase and Wallace 1986; Small and Anderson 1995). Alternatively, the absence of mantle lithosphere beneath the eastern Sierra Nevada and absence of a large crustal root imply that post-Miocene uplift is controlled primarily below the Moho (e.g., Crough and Thompson 1977; Wernicke et al. 1996; Liu and Shen 1998; Ruppert et al. 1998; Zandt et al. 2004).

The relationship between the rate of post-Miocene rock uplift and the rate of post-Miocene surface uplift (e.g., Small and Anderson 1995) is disputed. If the net vertical separation along the eastern frontal fault system since the Miocene is assumed to be 1–3 km (e.g., Wakabayashi and Sawyer 2001), then the corresponding increase in elevation is significantly less than the present peak elevation of 4419 m at Mount Whitney (Fig. 1), even without adjusting for erosion. Various models address this problem. Mean elevation may have decreased throughout the Cenozoic, despite post-Miocene uplift (Small and Anderson 1995; Wernicke et al. 1996; House et al. 2001). Alternatively, peak elevation may have increased since the late Miocene, but the magnitude and rate of increase are speculative (Huber 1981; Chase and Wallace 1986; Small and Anderson 1995; Wakabayashi and Sawyer 2001). The outcome of this debate is not critical to this study, but additional constraints on the relationship between arc dissection and physiographic evolution may help to explain certain ambiguities in sand(stone) composition trends (see Discussion and Mulch et al. 2006).

Active uplift is indicated by recent seismicity along the frontal fault system of the eastern Sierra Nevada (e.g., Ryall and Van Wormer 1980; Van Wormer and Ryall 1980; Zoback 1989; Ichinose et al. 1998; Ramelli et al. 1999). Sediment transport may be driven by surface uplift, but encroachment of the frontal fault system on the headwaters of west-flowing streams has limited their integration (Huber 1981; Wakabayashi and Sawyer 2001; Jones et al. 2004). Modern effects of rapid stream incision (e.g., Wakabayashi and Sawyer 2001) include meander entrenchment in the San Joaquin River canyon (Fig. 1) and rapid accumulation of Quaternary alluvium in the San Joaquin Valley (e.g., Huber 1981; Weissmann et al. 2002).

The complex history outlined above has resulted in diverse rock types in the Sierra Nevada and surrounding areas (Fig. 1). Compositions of sand in Sierra Nevada drainages are direct functions of the rock types in those drainages; these rock types, in turn, are direct functions of the tectonic history that created them. Thus, this study has the primary goal of testing the relation between sand composition and source-rock type, and the secondary goal of relating sand composition to plate-tectonic history, which has determined the rock types.

## PREVIOUS WORK

Compositions of sand(stone) derived from magmatic arcs indicate the degree to which the arcs (e.g., Sierra Nevada) have been dissected (Dickinson 1985; Marsaglia and Ingersoll 1992). Sand(stone) derived from active, undissected magmatic arcs is dominated by volcanic detritus; sand(stone) derived from inactive, dissected arcs is dominated by plutonic detritus. Magmatic arcs in transition from active volcanism to dissection yield transitional sand(stone) composition (Fig. 2).

Detrital modes of sand(stone) derived from undissected arcs yield a distinct volcanic signal (Dickinson 1985; Marsaglia and Ingersoll 1992). This signal is characterized by high ratios of plagioclase to total feldspar, low concentrations of quartz (Fig. 2), and varying concentrations of mica and accessory (dense) minerals. Lithic fragments (aphanitic polycrystalline grains of varying composition) are dominant (Fig. 2) and usually exhibit textures diagnostic of volcanic or hypabyssal origin (e.g., Kretchmer 1987; Ingersoll and Cavazza 1991; Marsaglia 1991; Marsaglia and Ingersoll 1992; Ingersoll et al. 1993).

In contrast, detrital modes of sand(stone) derived from dissected arcs represent a distinct plutonic signal (Dickinson 1985). This signal is characterized by lower ratios of plagioclase to total feldspar, relatively high concentrations of quartz and feldspar (Fig. 2), and varying concentrations of mica and accessory minerals. Monocrystalline grains are dominant; lithic fragments are subordinate (Fig. 2), with metamorphic or volcanic grains locally significant (Dickinson 1985).

Transitional arcs lie compositionally between volcanic-dominated (undissected) arcs and plutonic-dominated (dissected) arcs. As illustrated in Figure 1, complex combinations of volcanic, metamorphic, and plutonic rocks characterize transitional settings. These transitional settings (with their resulting transitional compositions) can develop through complex tectonic and erosional processes (Marsaglia 1991; Marsaglia et al. 1995). Arc dissection occurs when volcanism ceases, so

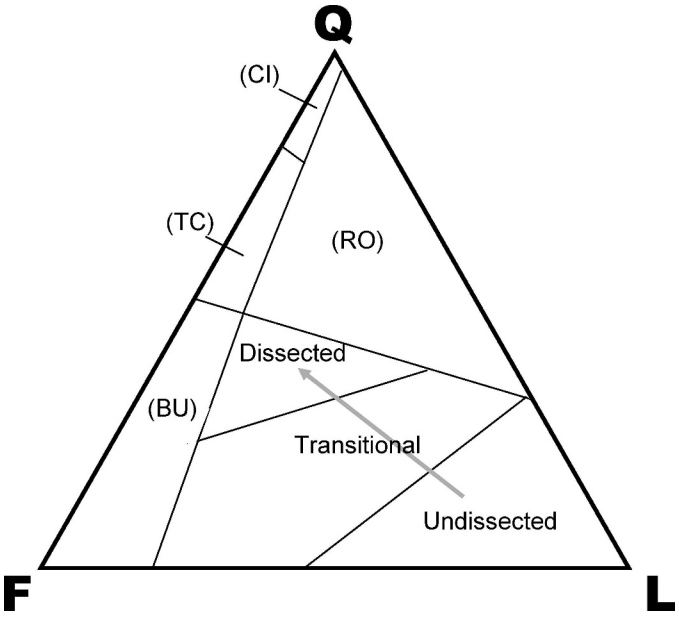


FIG. 2.—Ternary diagram showing provenance fields defined by total quartz (Q), total feldspar (F), and unstable (nonquartzose) lithic (L) sand(stone) composition. Designated fields refer to magmatic-arc provenance: undissected magmatic arc, transitional magmatic arc, and dissected magmatic arc. Gray arrow represents predicted trend for sand(stone) composition during arc dissection. Note progressive lithic depletion in transitional-arc and dissected-arc fields. Abbreviations represent provenance fields not directly associated with magmatic arcs (CI = craton interior, TC = transitional continental, RO = recycled orogenic, BU = basement uplift). After Dickinson (1985).

that erosional processes outpace eruptive processes. This may occur due to termination of magmatism following crustal collision (e.g., Schweickert and Cowan 1975), change in subducting-slab geometry (e.g., Keith 1978, 1982), or change in plate-margin type during triple-junction migration (e.g., Dickinson and Snyder 1979; Marsaglia 1991; Marsaglia et al. 1995). Termination of magmatism by any of these plate-tectonic processes results in gradual isostatic uplift as the volcanic cover is eroded, and metamorphic and plutonic rocks are exposed (Dickinson and Rich 1972; Ingersoll 1983; Dickinson 1985). More abrupt dissection occurs where tectonic forces rapidly uplift the entire arc terrane, as demonstrated by the southern Sierra Nevada (Fig. 1) and southern Baja California (Marsaglia 1991).

Traditionally, sedimentary petrologists have used ternary diagrams (e.g., Fig. 2) to analyze (sub)compositions of sand(stone). Ternary diagrams facilitate analysis of three variables in two-dimensional space and simplify interpretation of tectonic environment, diagenesis, and other aspects of sand(stone) composition. The use of ternary diagrams, however, can create statistical problems (Weltje 2002, 2004); construction of fields of variation is particularly problematic. For example, the use of summary statistics, such as arithmetic means and standard deviations, in the construction of such fields (e.g., Ingersoll 1978) yields different fields than does the construction of confidence regions (Weltje 2002, 2004).

The problem of sampling scale (the magnitude of sediment-dispersal systems) also must be recognized in studies of sand(stone) composition (Ingersoll 1990; Ingersoll et al. 1993). Higher sampling scale is assigned to integrated river systems with diverse rocks in their drainage; local streams constitute lower sampling scales. Grouping of specimens by sampling scale clarifies the effects of local complexity on regional or global (tectonic) sand(stone) provenance (Ingersoll 1990; Ingersoll et al. 1993). Ingersoll et al. (1993) documented that magmatic arcs provide uniform sand compositions at all sampling scales; thus, the use of Dickinson's third-order sampling model (Fig. 2) is justified for study of the first- and second-order samples of the present study.

## METHODS AND RESULTS

### *Specimen Treatment*

All sand specimens in this study ($n = 156$) were collected from streams in the Sierra Nevada and the southernmost Cascade Range, near Mount Lassen and Mount Shasta. The spatial distribution of the specimens (Fig. 1) represents diverse environmental conditions, including elevation (100–3,000 m), climate (arid to alpine), stream gradient, stream-flow conditions, and rock types (e.g., Fig. 1). No specimens from streams in the eastern Sierra Nevada draining the Bishop Tuff, a Tertiary volcanic unit thought to be unrelated to arc magmatism (Christensen 1966), were included. Data representing fifteen specimens from the southern Cascade Range were included from a previous study of similar scope and method (i.e., Kretchmer 1987).

All data included in this study represent specimens of similar sampling scale (e.g., Ingersoll 1990; Ingersoll et al. 1993). Specimens representing talus or small drainages composed of homogeneous rock type (Ia) were not included; a few specimens from integrated rivers that drain large areas of heterogeneous rock type (IIa) were included. Most of the specimens represent small drainages composed of heterogeneous rock type (Ib). Higher sampling scales (IIb and III) do not exist in the study area.

All specimens were dry-sieved in order to isolate sand grains (0.0625–2 mm). A portion of each specimen was mounted in epoxy and cut into a thin section, which was etched in concentrated HF and stained with sodium hexanitrocobaltate (III) for potassium-feldspar identification (e.g., Ingersoll and Cavazza 1991). Thin sections were point-counted using a mechanical advancing stage.

The Gazzi–Dickinson point-counting method is commonly used to determine the composition of sand(stones) in active tectonic settings (e.g., Ingersoll 1983; Ingersoll and Cavazza 1991; Marsaglia and Ingersoll 1992), because its use minimizes the effect of grain size on detrital modes (Ingersoll et al. 1984). The Gazzi–Dickinson method was used in counting 300 points per thin section; point-count categories ($n = 11$) are shown at the top of Table 1. Specimens with abundant organic matter and other intrabasinal components (e.g., Zuffa 1985) were not included. Most specimens contained minor intrabasinal material, which was ignored during the point-counting.

Raw data (Appendix 1 in JSR Data Archive, see Acknowledgments section), excluding mica, dense minerals, and miscellaneous-unknown grains, were recalculated to percentages with respect to QFL, QmFkFp, LmLvLs, and QpLvmLsm (e.g., Ingersoll et al. 1984; Dickinson 1985; Ingersoll 1990) (Appendix 2 in Data Archive). Raw data for mica and dense minerals were recalculated as percentages with respect to the point-count total of 300 (Appendix 2 in Data Archive). Ratios of plagioclase to total feldspar and polycrystalline quartz to total quartz were included. Each of the sixteen recalculated categories (e.g., Table 1) was analyzed for regional trends in two-dimensional scatter charts, using latitude as a preliminary variable. Selected scatter charts are shown in Figure 3.

### *Statistical Analyses*

**Discriminant Analysis.—**Statistical analysis of composition data involved several steps. All values of zero in the raw-data spreadsheet (Appendix 1 in Data Archive) were replaced with the lowest detectable limit of 0.5 to accommodate logarithmic transformation (e.g., Weltje 2002). All data were transformed to minimize statistical constraints (e.g., Weltje 2002). Raw point-count data contain inherent constraints that make rigorous analysis impractical. For example, every component abundance $x_i$ (where $x_i$ represents the abundance of any of the original eleven categories in Table 1) is non-negative. Also, in any given 300-point

TABLE 1.—*Definition of Point-Count Categories.*

| | |
|---|---|
| COUNTED PARAMETERS | |
| Qm | Monocrystalline quartz |
| Qp | Polycrystalline quartz |
| Fp | Plagioclase feldspar |
| Fk | Potassium feldspar |
| Lmv | Metavolcanic lithic |
| Lms | Metasedimentary lithic |
| Ls | Sedimentary lithic |
| Lv | Volcanic-hypabyssal lithic |
| M | Phyllosilicate (mica) minerals |
| D | Dense (accessory) minerals |
| Misc | Miscellaneous or unidentified |
| OTHER ABBREVIATIONS | |
| Q = Qm + Qp | Total quartzose grains |
| F = Fp + Fk | Total feldspar grains |
| L = Lm + Lv + Ls | Unstable (nonquartzose) lithic grains |
| Lm = Lmv + Lms | Metamorphic lithic grains |
| Lvm = Lv + Lmv | Volcanic-hypabyssal and metavolcanic lithic grains |
| Lsm = Ls + Lms | Sedimentary and metasedimentary lithic grains |
| RECALCULATED PARAMETERS AND RATIOS | |
| QFL%Q = 100 × Q/(Q + F + L) | LmLvLs%Lm = 100 × (Lm/L) |
| QFL%F = 100 × F/(Q + F + L) | LmLvLs%Lv = 100 × (Lv/L) |
| QFL%L = 100 × L/(Q + F + L) | LmLvLs%Ls = 100 × (Ls/L) |
| QmFkFp%Qm = 100 × Qm/(Qm + Fk + Fp) | QpLvmLsm%Qp = 100 × Qp/(L + Qp) |
| QmFkFp%Fk = 100 × Fk/(Qm + Fk + Fp) | QpLvmLsm%Lvm = 100 × Lvm/(L + Qp) |
| QmFkFp%Fp = 100 × Fp/(Qm + Fk + Fp) | QpLvmLsm%Lsm = 100 × Lsm/(L + Qp) |
| %D = 100 × D/300 | Fp/F = Fp/(Fp + Fk) |
| %M = 100 × M/300 | Qp/Q = Qp/(Qp + Qm) |

count, the sum of the components is fixed at 300:

$$\sum_{i=1}^{k} x_i = 300,\ x_i \geq 0. \tag{1}$$

Therefore, the abundance value of the $k$th component is constrained by the sum of the remaining values:

$$x_k = 300 - \sum_{i=1}^{k-1} x_i. \tag{2}$$

These constraints prevent the values of $x_i$ from varying independently. Both constraints are removed through logratio transformation (e.g., Weltje 2002), in which all values of $x_i$ are divided by the corresponding value of the $k$th component, and the logarithm $y$ of each ratio (excluding $x_k/x_k$) is calculated:

$$y_i = \log\left(\frac{x_i}{x_k}\right), \text{where} i = 1,2,...,k-1. \tag{3}$$

Monocrystalline quartz (Qm) was selected to represent the $k$th component, such that all other values were divided by the corresponding value of Qm. The logarithm of each ratio was calculated accordingly. Discriminant analysis was applied to the logratio transformation of the data set using Systat software (SPSS 2000).

The purpose of discriminant analysis is to classify multivariate observations into mathematically defined groups (e.g., Koch and Link 1971). This procedure optimally clusters the data as ellipsoidal clouds in multidimensional space, such that the directions and lengths of the distances connecting ellipsoid centers maximize the spatial distinction (or separation, or discrimination) among the groups (Koch and Link 1971). Discriminant analysis modifies the statistical concept of univariate distance $d$,

$$d = \frac{\overline{w}_1 - \overline{w}_2}{s}, \tag{4}$$

where $\overline{w}_1$ and $\overline{w}_2$ represent mean values of two samples with equal standard deviation $s$, to apply to multivariate data. In the relatively simple case of bivariate data, modification depends on whether the variables are correlated or uncorrelated. If the variables are uncorrelated, then Equation 4 is combined with the equation for geometric distance between two points in Cartesian coordinates, $a^2 = b^2 + c^2$, to yield:

$$d = \sqrt{\frac{(\overline{w}_{11} - \overline{w}_{12})^2}{\sigma_{w1}^2} + \frac{(\overline{w}_{21} - \overline{w}_{22})^2}{\sigma_{w2}^2}}, \tag{5}$$

where $\sigma$ represents the standard deviation of a given sample. Alternatively, if the variables are correlated, then:

$$d^2 = a(\overline{w}_{11} - \overline{w}_{12})^2 + 2b(\overline{w}_{11} - \overline{w}_{12})(\overline{w}_{21} - \overline{w}_{12}) + c(\overline{w}_{21} - \overline{w}_{22})^2, \tag{6}$$

where $a$, $b$, and $c$ represent elements of the inverse matrix $\mathbf{A}^{-1}$ of the covariance matrix $\mathbf{A}$ (Koch and Link 1971). Large values of $d$ represent greater statistical distance, or discrimination, between a pair of samples. For a comprehensive explanation of discriminant analysis, the interested reader is referred to Koch and Link (1971) and Tabachnick and Fidell (2001).

Note the $d^2$ notation, instead of $d$, in Equation 6. Complex multivariate data sets (as opposed to the simple bivariate case) are measured for statistical distinction by a criterion known as Mahalanobis' $d^2$ statistic, or $D^2$ statistic (commonly abbreviated "Mahal" or $D^2$). This value is based on the distance between pairs of group centroids, generalized to distances over multiple pairs of groups (Tabachnick and Fidell 2001). Other measurements of statistical distinction (e.g., Wilks' lambda and approximate F value) are also used. Discriminant analysis is complete when statistical distinction is maximized.

Discriminant analysis is a special case of *canonical correlation*, which closely resembles multiple regression in its description (Tabachnick and Fidell 2001). In multiple regression, a single variable on one side of the regression equation is determined by a series of variables on the other:

$$Y' = A + B_1X_1 + B_2X_2 + ... + B_kX_k, \tag{7}$$

where $Y'$ is the predicted value of $Y$, $A$ is the $y$ intercept, $B_1$ to $B_k$ represent regression coefficients, and $X_1$ to $X_k$ represent the independent variables (Tabachnick and Fidell 2001). The column matrix **B** (commonly denoted $\mathbf{B}_i$) represents a series of regression coefficients, such that Equation 7 minimizes the sum of squared residuals (i.e., differences between $Y$ and $Y'$). In canonical correlation, the objective is similar to that of multiple regression (i.e., derivation of a series of coefficients that yield an optimal result), but there are multiple variables on both sides of the equation (Tabachnick and Fidell 2001). In a plot of a canonical function in Cartesian coordinates, the axes represent canonical variates, or factors composed of multiple variables. Variates are defined by a series of coefficients that maximize statistical distinction.

The Systat application combines these principles of discriminant analysis and canonical correlation to generate a grid that represents ellipsoidal clouds of optimally separated points in two-dimensional space (e.g., Fig. 4). Three variates ("factors" in Fig. 4) are represented as axes. Pairings of variates are shown in individual cells of the grid, and each pairing reveals the elliptical cross section of the ellipsoidal cloud in the

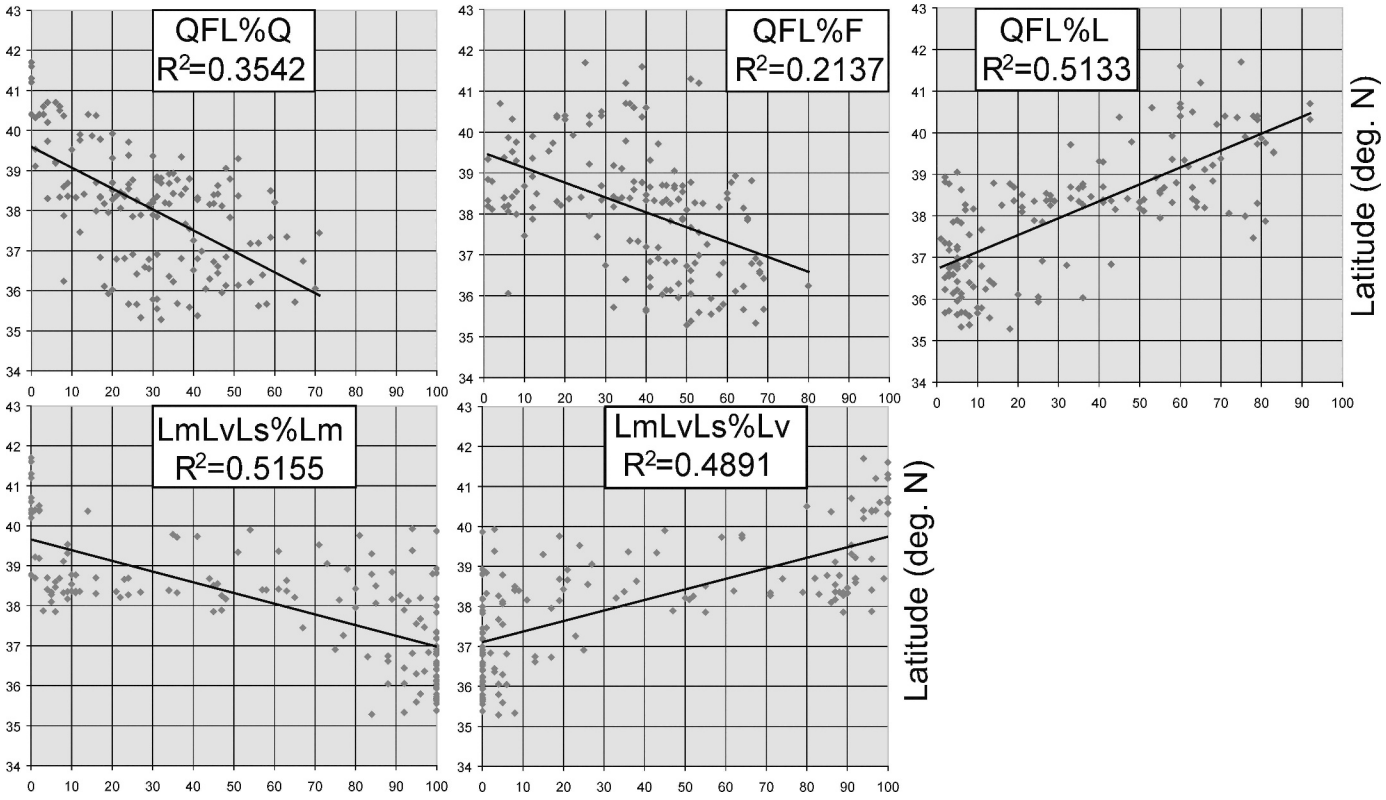


FIG. 3.— Bivariate plots of selected recalculated parameters (horizontal axes) (see Table 1) versus latitude (vertical axes). QFL%Q, QFL%F, and LmLvLs%Lm decrease with increasing latitude, whereas QFL%L and LmLvLs%Lv increase with increasing latitude. Increasing latitude correlates with decreasing arc dissection (see Figs. 1, 2).

corresponding plane. Confidence ellipses are defined by the resulting scatter of points determined by the pair of equations that comprise the variates. Each of the cells that form the main diagonal of the grid represents one of the variates (e.g., Factor[1] in the upper left), with point frequency as the vertical axis (analogous to univariate frequency curves, such as the curve implicit in Equation 4).

**Analysis of Sierra Nevada Data.—**Based on Figure 3, specimens were sorted into three preliminary data groups, defined by lines of latitude (37 and 40 degrees), that correspond roughly with transitions in overall rock types (e.g., Fig. 1). Discriminant analyses using these groupings supported additional sorting of the intermediate group, which was replaced, initially, by multiple groups; subsequent discriminant analyses indicated two subgroups within the intermediate group: "plutonic-volcanic" (or "transitional") and "plutonic-metamorphic" ("dissected"). Four data groups were included in the final analysis: Undissected (*U*), Transitional (*T*), Dissected (*D*), and Basement (*B*) (Table 2).

The initial Systat discriminant analysis showed that preliminary assignment of the specimens based on latitude roughly classified the specimens. On the other hand, some of the specimens in each group were clearly discordant. The assignment of most discordant specimens was corrected through seven iterations of discriminant analysis. The analysis calculated the contribution of each petrographic variable to the statistical distinction among the groups. For example, Table 3 shows that LvLogRat contributed most to group discrimination in the final analysis. As expected, the canonical factor that depended mainly on the log ratio of Lv (Table 4) separated the data groups most effectively. For each iteration, the weakest parameter(s) (i.e., the parameter[s] that contributed least to separation of the groups) was (were) removed from the analysis automatically. In the final analysis (Tables 3 and 4), the only variable that did not contribute significantly was the log ratio of *D* (dense-mineral content).

The number of specimens "correctly" assigned to each group was tallied with each iteration. Table 5 shows the tally of the final analysis. Any specimen that was not correctly assigned to a group was identified by the analysis and reviewed individually, as follows: (1) for each discordant specimen, the values for the strongest variables were compared with the calculated central values for each group (Table 6); (2) if the values for the strongest variables closely resembled the central values of another group (Table 6), then the specimen was reassigned to the other group; (3) if the new group assignment was not warranted by the specimen location (e.g., the analysis suggested that a low-latitude specimen be removed from the Basement group), then the reassignment was cancelled. In other words, latitude was used as an informal grouping parameter.

Iteration of the discriminant analysis clustered specimens of similar composition into four groups (*U*, *T, D*, and *B*) and effectively removed the variable of latitude from the definition of the groups. Iteration continued until specimen reassignment yielded no improvement in the correlation ("total % correct" of Table 5) of the specimens to group means (Table 6). Ultimately, four outliers in *T* and *D* remained (Table 5) among 156 specimens; *U* and *B* contain no outliers. The final canonical plot (Fig. 5) shows the canonical-score cluster, by group, as opposed to the recalculated raw-data scatter versus latitude in Figure 3, which only partially represents the compositional data of each specimen.

Additional discriminant analysis was performed on the entire data set, sorted by specimen location relative to the drainage divide (Fig. 1). This replaced the four latitudinal groups with two drainage groups, "east" (*e*) and "west" (*w*) (Appendix 3 in Data Archive). With the data sorted east–

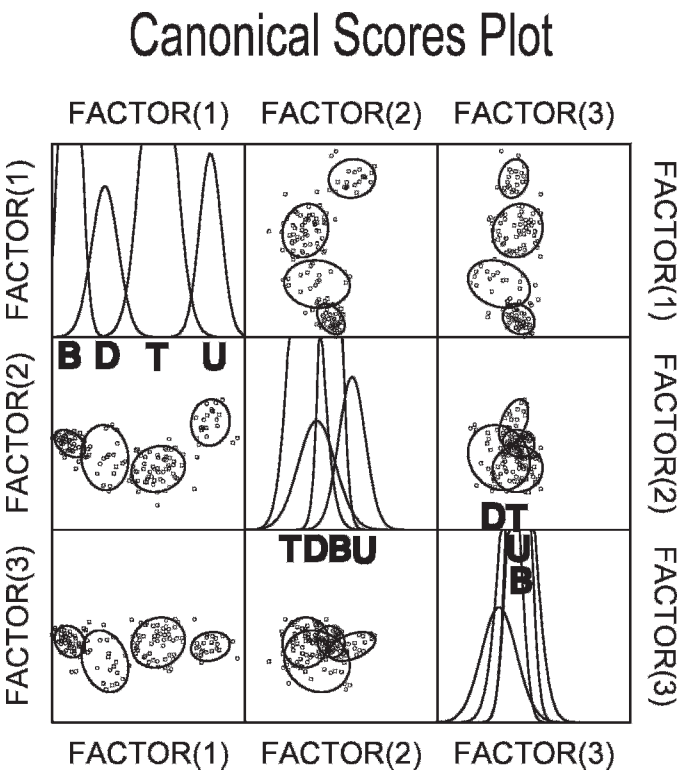


FIG. 4.—Canonical scores plot of discriminant analysis (SPSS, 2000). Data used to construct canonical scores grid represent final iteration of Systat application. See Figure 5 for enlargement of Factor 2 versus Factor 1 (left-center cell in this figure). Total points = 156. Grid layout substitutes for three-dimensional diagram and shows all possible pairings of canonical variates Factor 1, Factor 2, and Factor 3. Ellipses showing 68% confidence limits represent cross sections of ellipsoidal clouds generated by discriminant analysis. In each grid cell containing confidence ellipses, selected canonical variates comprise horizontal and vertical axes. Note resemblance of cells that share identical axes. For example, in the left-center cell, Factor 1 is represented as the horizontal axis and Factor 2 is represented as the vertical axis; in the top-center cell, Factor 2 is represented as the horizontal axis and Factor 1 is represented as the vertical axis. Cells containing frequency curves represent cross-sections of ellipses in corresponding columns. The vertical axis of each bell-curve cell represents the score frequency of the corresponding variate, analogous to univariate frequency curves (compare Equation 4). Frequency-curve cells emphasize the contribution of each canonical variate to separation of groups (U, T, D, and B). Note significant separation in Factor 1 cell (upper left) relative to Factor 2 cell (center) and Factor 3 cell (lower right). Total number of points in each group corresponds to totals listed in Table 5. Group means for each factor are shown in Table 6. Group labels (B, D, T, and U) are shown below or above the mean value for each bell curve.

west, potassium feldspar was the strongest variable in the discriminant analysis (Tables 7 and 8). The specimens were not reassigned, and the drainage groups were not adjusted for statistical affinity (Table 9). Comparison of the "total % correct" values in Tables 5 and 9 shows that the drainage groups (east and west) are not as significant, statistically, as the arc-dissection groups. Nonetheless, these drainage groups show that significant compositional contrasts exist across the Sierra Nevada arc, especially the systematic increase in potassium feldspar from west to east (Kistler and Peterman 1973; Keith 1982; Ingersoll 1983; Linn et al. 1992).

The canonical plot in Figure 5 clearly differentiates among the four groups, without overlap of confidence ellipses at the 68% (one standard deviation) confidence limit. The canonical plot is a two-dimensional representation of multidimensional space. Unlike in ternary plots (Figs. 6, 7) and scatter charts (Fig. 3), none of the variables shown in Table 2 is represented exclusively by either axis of the canonical plot. All of the variables in Table 4 contribute to definition of both canonical factors (i.e., Factor[1] and Factor[2] of Fig. 5) to some degree.

Figure 5 reflects the important contribution of LmLvLs%Lv in separation of the groups (Table 5). The horizontal axis represents the strongest canonical variable and is heavily dependent on LmLvLs%Lv (Table 4). Figure 5 and Table 6 show that canonical scores for Factor 1 are very positive in *U*, slightly positive in *T*, slightly negative in *D*, and very negative in *B*.

Figure 5 and Table 6 also indicate the important contribution of QmFkFp%Fp (Table 3). Canonical scores for Factor 2, which reflects the contribution of QmFkFp%Fp most strongly (Table 4), tend to be very positive in *U*, slightly positive in *B*, slightly negative in *D*, and more negative in *T*. Figure 5 shows that the separation produced by Factor 2 is more ambiguous than that produced by Factor 1. The vertical range of each confidence ellipse is overlapped by the vertical range of every other group, except for *U* and *T*.

### *Ternary Diagrams*

Recalculated summary statistics for each of the final arc-dissection groups (*U*, *T*, *D*, and *B*) (Table 2) were used to construct confidence regions (Weltje 2002) (Fig. 6) and hexagonal fields of variation (Ingersoll 1978) (Fig. 7). Hexagonal fields of variation (e.g., Ingersoll 1978), defined by the standard deviation or other specified quantity about the mean in each direction, involve statistical ambiguities that are eliminated with the use of confidence regions (Weltje 2002). An additional problem with hexagonal fields is demonstrated in Table 2 and in Figure 7, in which the sum of a given arithmetic mean and corresponding standard deviation may exceed the 100-percent range of a ternary diagram. For example, in *U*, all standard-deviation values for the QmFkFp data, when added to or subtracted from the corresponding mean value, yield at least one value that is either less than zero or greater than unity (100 percent). Limits of each variable, when represented as hexagons, would plot partly beyond the area of the ternary diagram, if shown in Figure 7.

The summary statistics (Table 2) are consistent with previous descriptions of magmatic-arc compositions (e.g., Dickinson 1985; Marsaglia and Ingersoll 1992) (Figs. 6, 7). Sand from the undissected, northern Sierra Nevada is dominated by volcanic lithic fragments, with high ratios of plagioclase to total feldspar. Sand from the dissected, southern Sierra Nevada is depleted in lithic fragments relative to quartz and feldspar, with relatively high ratios of potassium feldspar to total feldspar. Extreme lithic depletion in the southern Sierra Nevada places the provenance field of *B* in the basement-uplift field. The intermediate groups also support the general trend of lithic depletion with decreasing latitude (Figs. 3, 6, 7).

Data from *T* and *D* show that the "transitional" signal predicted in Figure 2 is complex (Figs. 6, 7). For example, relative concentrations of several components, such as QmFkFp%Qm, QmFkFp%Fp, and LmLvLs%Ls, conspicuously peak or plunge, relative to the regional "trend," in at least one of the intermediate groups (Table 2). Other components, such as QFL%F, Fp/F, and %D, reflect stronger correlation between the intermediate groups and one of the end-member groups than might be expected from a zone of "transition." With respect to all of these components, the intermediate groups do not constitute a zone of simple compositional gradation between volcanic and plutonic end members. The two intermediate groups can be defined as much by distinctive proportions of metamorphic and other components as they are by intermediate compositional values for "critical" variables (Table 3), such as volcanic lithics and plagioclase. On the other hand, some trends in the intermediate groups are consistent with the "transition" label (Table 2). QpLvmLsm%Lsm, LmLvLs%Lm, and %M all increase regularly from north to south, as implied by Dickinson's (1985) arc-dissection model.

Similarity between confidence regions (Fig. 6) and hexagonal fields of variation suggest that summary statistics (Table 2) can be used to

TABLE 2.—*Summary statistics of compositional data, showing arithmetic means and standard deviations of recalculated parameters (see Table 1).*

| | *U* | | *T* | | *D* | | *B* | |
|---|---|---|---|---|---|---|---|---|
| | Mean | StdDv | Mean | StdDv | Mean | StdDv | Mean | StdDv |
| Qp/Q | 0.02 | 0.05 | 0.02 | 0.05 | 0.02 | 0.07 | 0 | 0.10 |
| Fp/F | 0.99 | 0.05 | 0.70 | 0.21 | 0.70 | 0.22 | 0.68 | 0.11 |
| QmFkFp%Qm | 12 | 13 | 45 | 23 | 63 | 23 | 41 | 13 |
| QmFkFp%Fk | 1 | 4 | 14 | 9 | 9 | 8 | 19 | 7 |
| QmFkFp%Fp | 87 | 14 | 41 | 21 | 27 | 20 | 40 | 11 |
| QFL%Q | 4 | 4 | 25 | 14 | 37 | 16 | 38 | 14 |
| QFL%F | 29 | 12 | 31 | 18 | 27 | 23 | 53 | 11 |
| QFL%L | 67 | 13 | 44 | 20 | 36 | 30 | 9 | 8 |
| QpLvmLsm%Qp | 0 | 1 | 1 | 4 | 3 | 7 | 1 | 3 |
| QpLvmLsm%Lvm | 96 | 5 | 66 | 27 | 28 | 23 | 9 | 9 |
| QpLvmLsm%Lsm | 4 | 4 | 33 | 26 | 70 | 22 | 89 | 9 |
| LmLvLs%Lm | 1 | 2 | 34 | 29 | 84 | 18 | 98 | 5 |
| LmLvLs%Lv | 96 | 5 | 60 | 32 | 10 | 15 | 2 | 4 |
| LmLvLs%Ls | 3 | 4 | 6 | 11 | 6 | 15 | 1 | 2 |
| %M | 0.30 | 0.60 | 2.10 | 2.00 | 2.90 | 2.60 | 3.80 | 2.80 |
| %D | 11.00 | 8.30 | 5.00 | 3.70 | 4.90 | 4.10 | 4.70 | 4.90 |

*U* = undissected, *T* = transitional, *D* = dissected, *B* = basement

TABLE 3.—*Canonical variable strength.*

| Variable | F-to-remove | Tolerance |
|---|---|---|
| LvLogRat | 247.73 | 0.293471 |
| FpLogRat | 46.54 | 0.235021 |
| LmsLogRat | 18.76 | 0.308876 |
| FkLogRat | 12.79 | 0.588806 |
| QpLogRat | 9.51 | 0.604275 |
| LmvLogRat | 6.00 | 0.382220 |
| LsLogRat | 5.04 | 0.712654 |
| MLogRat | 4.21 | 0.560164 |
| MiscLogRat | 3.33 | 0.438284 |
| Variable | F-to-enter | Tolerance |
| DLogRat | 0.74 | 0.353882 |

generate reliable fields of compositional variation. This similarity, however, is insufficient to support use of hexagonal fields in statistically rigorous analysis of sand(stone) composition. Comparison of arithmetic means for the QFL series in *D* (Table 2) (Fig. 7) with geometric means in Figure 6 shows that logratio data may yield significantly different mean values than untransformed data (Weltje 2002, 2004). Therefore, the geometric means of each group in Figure 6 do not correspond with arithmetic means in Figure 7. Implicitly, sand(stone) data from previous studies should be used to generate geometric means and confidence

TABLE 4.—*Canonical discriminant functions.*

| | Factor 1 | Factor 2 | Factor 3 |
|---|---|---|---|
| QpLogRat | 0.497 | 1.486 | 0.179 |
| FkLogRat | −0.423 | −1.071 | 1.680 |
| FpLogRat | −1.608 | 2.594 | 0.286 |
| LmvLogRat | 0.666 | −0.184 | −0.932 |
| LmsLogRat | −1.417 | −0.788 | 0.450 |
| LvLogRat | 3.115 | −1.419 | 0.373 |
| LsLogRat | 0.134 | 0.823 | −0.166 |
| MLogRat | 0.518 | −0.671 | −0.901 |
| MiscLogRat | −0.755 | 0.194 | −0.022 |

TABLE 5.—*Group-classification matrix.*

| | *B* | *D* | *T* | *U* | Total | % correct |
|---|---|---|---|---|---|---|
| *B* | 51 | 0 | 0 | 0 | 51 | 100 |
| *D* | 2 | 20 | 0 | 0 | 22 | 91 |
| *T* | 0 | 1 | 59 | 1 | 61 | 97 |
| *U* | 0 | 0 | 0 | 22 | 22 | 100 |
| Total % correct (affinity): | | | | | | 97 |

regions that are comparable to arithmetic means and fields presently in use. One type of data cannot be used to test models based on the other type of data. For example, Figure 8 illustrates the lack of correspondence of geometric mean and confidence interval of *D* with the Dissected Arc field of Dickinson (1985), whereas the arithmetic mean of the same data plots within the predicted field. This lack of correspondence does not negate Dickinson's model; rather it demonstrates the need for methodological consistency in model testing.

## DISCUSSION

The final canonical plot (Fig. 5) justifies grouping by latitude as a preliminary criterion, even though emphasis on latitude (e.g., Fig. 3) is removed in the final analysis (Table 5). Sand composition and latitude are highly correlated in the Sierra Nevada, as predicted by northward migration of the southern end of the active magmatic arc and rapid uplift of the southern Sierra Nevada during the late Cenozoic (Dickinson and Snyder 1979; Dickinson 1997; Atwater and Stock 1998).

The results of this study are broadly consistent with Dickinson's (1985) model (Fig. 2), whether one uses raw data, recalculated ternary ratios, log

TABLE 6.—*Canonical scores of group means.*

| | Factor 1 | Factor 2 | Factor 3 |
|---|---|---|---|
| *B* | −4.611 | 0.697 | 0.300 |
| *D* | −1.887 | −0.393 | −1.230 |
| *T* | 2.260 | −1.284 | 0.221 |
| *U* | 6.311 | 2.338 | −0.078 |

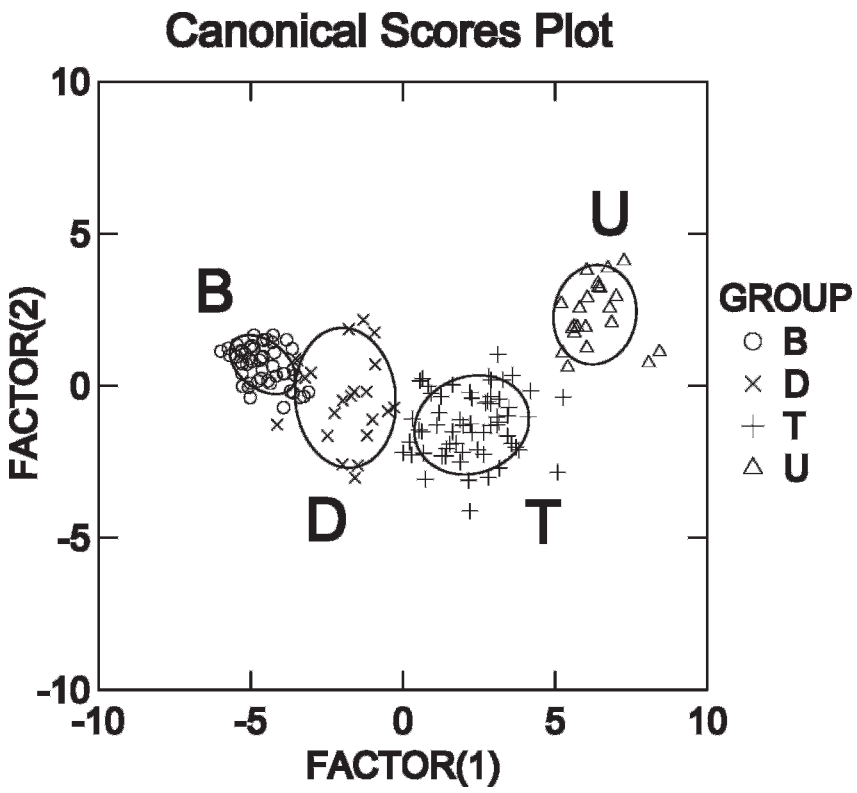


FIG. 5.—Simplified canonical plot of discriminant analysis. The left-center cell of grid shown in Figure 4 is enlarged to show the scale of both axes (Table 6). Ellipses represent 68% confidence limits of each group of scores. The separation of ellipses is determined primarily by Factor 1, which corresponds with the horizontal axis. Vertical ranges of ellipses tend to overlap. Factor 1 is strongly dependent on volcanic-lithic content (Tables 3 and 4). Factor 2 is strongly dependent on plagioclase content. Note the clear distinction between horizontal ranges of end-member groups U and B, and compare separation patterns in Figure 6, which primarily reflects volcanic-lithic content. Total points = 156: U ($n$ = 22), T ($n$ = 61), D ($n$ = 22), and B ($n$ = 51).

data, or log-ratio data. Certain results, such as the complex composition of *D*, are not predicted by previous models; rather, they reflect the complex local geology. Most of the Sierra Nevada (Fig. 1) is composed of volcanic and plutonic rocks associated with continental-arc magmatism. Exposure of metavolcanic and metasedimentary rocks is most widespread in the western Sierra Nevada (Fig. 1), where accretion and suturing occurred during the Nevadan orogeny (e.g., Schweickert and Cowan 1975; Ingersoll 1997, 2000; Godfrey and Klemperer 1998). Young volcanic cover in the north (Fig. 1) prevents this potential metamorphic detritus from contaminating *U* (Figs. 6, 7). In the southern Sierra Nevada, extreme uplift and erosion of accreted terranes, and general exposure of the batholith are such that *B* is mostly uncontaminated by metamorphic lithics as well (Fig. 6).

Extreme depletion of lithic fragments in *B* (Figs. 6, 7) is not predicted by the arc-dissection path (Fig. 2). Dickinson's (1985) model interprets the QFL compositions of *B* to be indicative of basement uplift, such as a rift shoulder or transform rupture. Either Dickinson's model is limited in interpreting the end stages of arc dissection, or the extreme lithic depletion is indicative of tectonic processes unrelated to "normal" arc dissection. In either case, sand composition from the present study is consistent with extreme uplift of the southern Sierra Nevada, resulting from complex Cenozoic tectonics.

This raises the general question of whether geologic process should be recognized based on (1) evolutionary *path* in QFL space, or (2) terminal composition. For example, the evolutionary trend of Sierra Nevada sand (Figs. 6, 7) initially matches the predicted path for arc dissection (Fig. 2). The arc-dissection model, however, implies that dissection is complete when depletion of lithic fragments produces sand composition consistent with the dissected-arc field, near the center of the QFL diagram. Subsequent evolution of sand composition, from the center of the diagram toward a different provenance field, such as the basement-uplift field of Figure 2, implies an additional process, such as extreme uplift of the batholith.

Alternatively, if geologic process is recognized based on terminal-phase composition, then the process responsible for generating the sand of the southern Sierra Nevada would be "basement uplift" or "rifting," not "arc dissection." In the sense that the Basin and Range constitutes a modified continental rift (e.g., Leeder and Gawthorpe 1987; Leeder 1995; Dickinson 2002), the Sierra Nevada should be considered a modified rift shoulder. Independent evidence from the southern Sierra Nevada (e.g., Saleeby et al. 1987, 2003; Wernicke et al. 1996; House et al. 2001; Jones et al. 2004) suggests that late Cenozoic uplift and dissection have been

TABLE 7.—*Canonical variable strength, east-west classification.*

| Variable | F-to-remove | Tolerance |
|---|---|---|
| FkLogRat | 27.52 | 0.576608 |
| MLogRat | 8.06 | 0.493170 |
| DLogRat | 5.97 | 0.171053 |
| LmvLogRat | 4.56 | 0.554908 |
| FpLogRat | 3.57 | 0.201242 |
| LvLogRat | 2.80 | 0.382358 |
| Variable | F-to-enter | Tolerance |
| LsLogRat | 1.05 | 0.330787 |
| MiscLogRat | 1.02 | 0.356713 |
| QpLogRat | 0.71 | 0.358221 |
| LmsLogRat | 0.65 | 0.451149 |

TABLE 8.—*Canonical discriminant functions, east-west classification.*

| | Factor 1 |
|---|---|
| FkLogRat | 1.905 |
| FpLogRat | 0.810 |
| LmvLogRat | 0.516 |
| LvLogRat | 0.271 |
| DLogRat | −1.035 |
| MLogRat | −1.194 |

TABLE 9.—*Group classification, east-west classification.*

| | *e* | *w* | Total | % correct |
|---|---|---|---|---|
| *e* | 31 | 11 | 42 | 74 |
| *w* | 29 | 85 | 114 | 75 |
| Total % correct: | | | | 74 |

extreme, and unrelated to typical arc dissection. The question is not whether sand(stone) composition of the southern Sierra Nevada is controlled mainly by "uplift" or by "dissection," but whether these processes can be distinguished solely on the basis of QFL paths. In the case of the Sierra Nevada, it seems that unusual tectonic uplift has modified the typical dissection process, and that this contrast with typical arc dissection is reflected in sand composition. Marsaglia (1991) documented similar extreme arc dissection in southern Baja California, also related to rifting resulting from triple-junction interactions (e.g., Ingersoll 1982).

## CONCLUSIONS

The process of arc dissection is evident in the composition of modern sand from the Sierra Nevada, where latitudinal position (north to south) can be used as proxy for temporal compositional trends (undissected arc through basement uplift). Multivariate statistical analysis supports classification of Sierra Nevada sand as "undissected," "transitional," and "dissected magmatic arc," with a quartzofeldspathic "uplifted-basement" suite representing the southernmost samples. The results of this study are consistent with Dickinson's arc-dissection model.

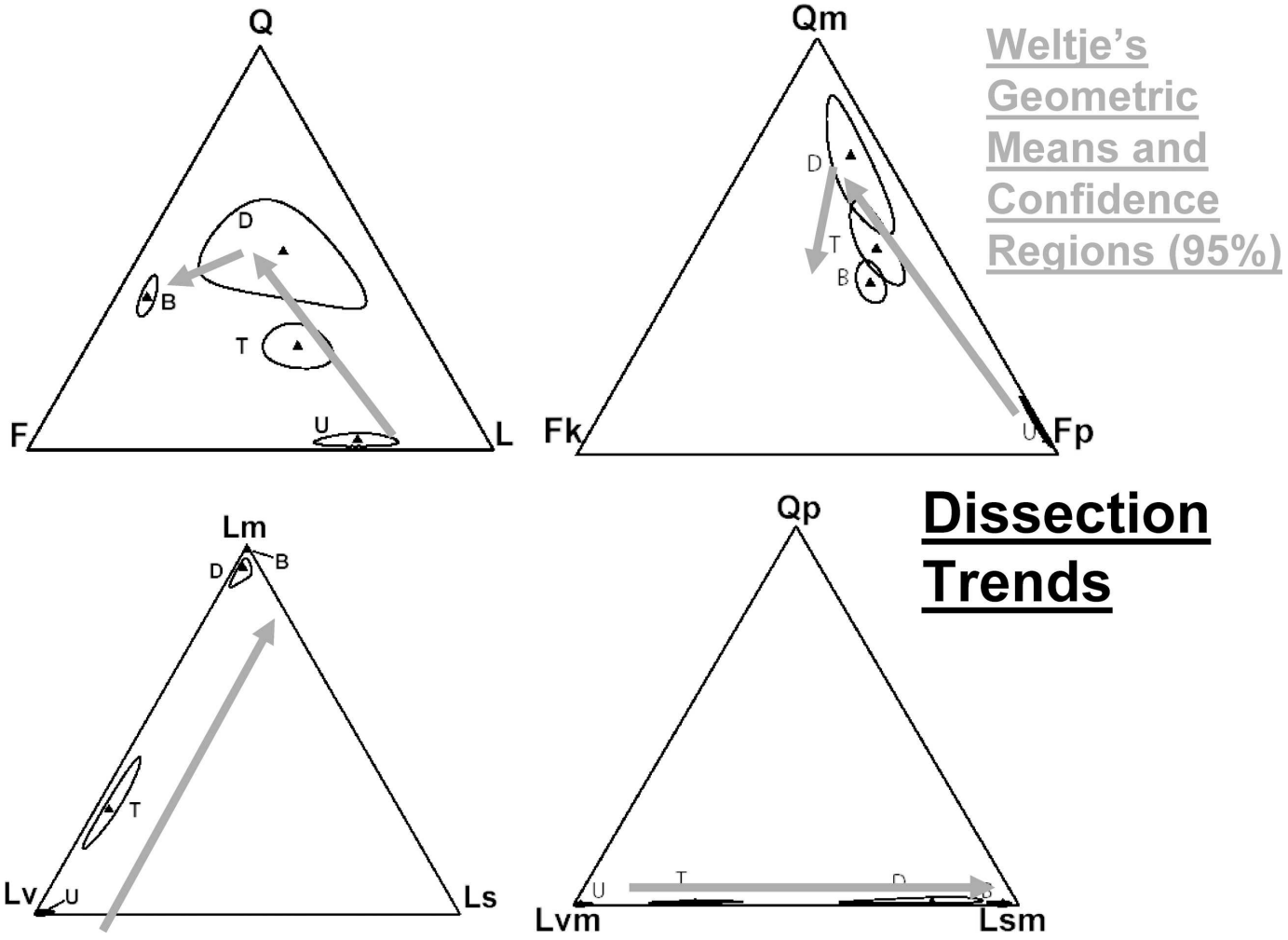


FIG. 6.—Ternary diagrams showing geometric means and their 95% confidence regions for each group (Weltje 2002). Also shown are general dissection trends represented by the four groups (from north to south; see Fig. 1). See Table 1 for definitions and recalculations, and Table 2 in Data Archive for recalculated parameters.

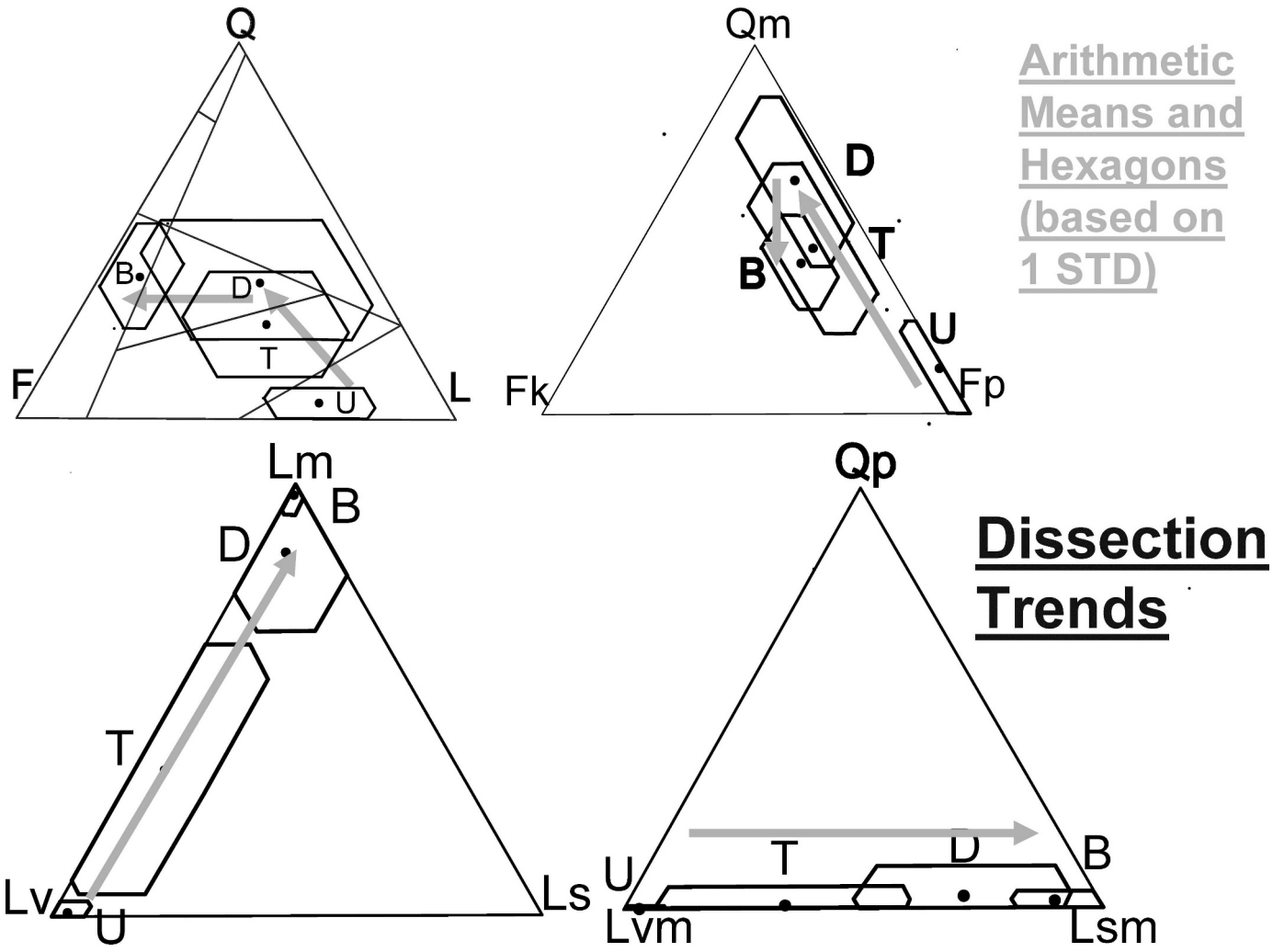


FIG. 7.— Ternary diagrams showing arithmetic means and hexagons based on 1 standard deviation for each parameter (Ingersoll 1978). QFL diagram contains provenance fields of Dickinson (1985) (see Fig. 2). Also shown are general dissection trends represented by the four groups (from north to south; see Fig. 1). See Table 1 for definitions and recalculations, and Table 2 in Data Archive for recalculated parameters.

Compositions of samples from the transitional and dissected groups are complex, reflecting paleotectonic conditions of the Sierra Nevada region, as well as degree of dissection. Exposure of diverse rock types, including Paleozoic and Mesozoic metamorphic terranes, and Cenozoic volcanic cover, is a source of complexity with respect to compositional trends in both groups.

No point-count parameter is "diagnostic" of arc dissection, although volcanic-lithic content is highly negatively correlated with degree of arc dissection. In the Sierra Nevada, compositional trends are such that certain parameters (e.g., dense-mineral content) are statistically irrelevant. In contrast, volcanic-lithic and plagioclase content contribute significantly to the statistical separation of undissected, transitional, dissected, and basement groups. The volcanic-lithic trend best distinguishes each group and limits ambiguity in the regional compositional trend. The extreme lithic depletion of the southernmost Sierra Nevada is due to its present position as the western rift shoulder of the Basin and Range.

The primary drainage divide of the Sierra Nevada represents a rough compositional boundary between "eastern" and "western" dissected arc. The primary discriminating factor between "eastern" and "western" composition is potassium feldspar, which is higher in the east. These drainage groups are not as statistically distinct as the arc-dissection groups.

Use of logratio transformed data provides additional rigor to discriminant and other statistical analyses. The use of confidence intervals (e.g., Weltje 2002, 2004) and the hexagon method of constructing confidence regions (e.g., Ingersoll 1978, 1983) on ternary plots produce similar graphical representations, although Weltje's method provides more opportunity for rigorous analysis. Weltje's mean population values cannot be used on ternary plots constructed using arithmetic means (e.g., Dickinson 1985; Marsaglia and Ingersoll 1992). Consistent petrographic and statistical methods must be utilized during tests of compositional models.

#### ACKNOWLEDGMENTS

We thank Jenny Ingersoll and Jennifer Cadkin for help in collecting and processing sand samples. We also thank Andrea Kretchmer for supplementing the point-count data set in the Cascade Range, and Gary Axen and Brian Horton for reviewing earlier versions of this manuscript. Gary Girty, Bill Heins and Kathie Marsaglia provided helpful and thoughtful reviews of the JSR manuscript. Financial support was provided by the California Science Project and the Council on Research of the Academic Senate of the Los Angeles Division of the University of California. Appendices 1–3 are

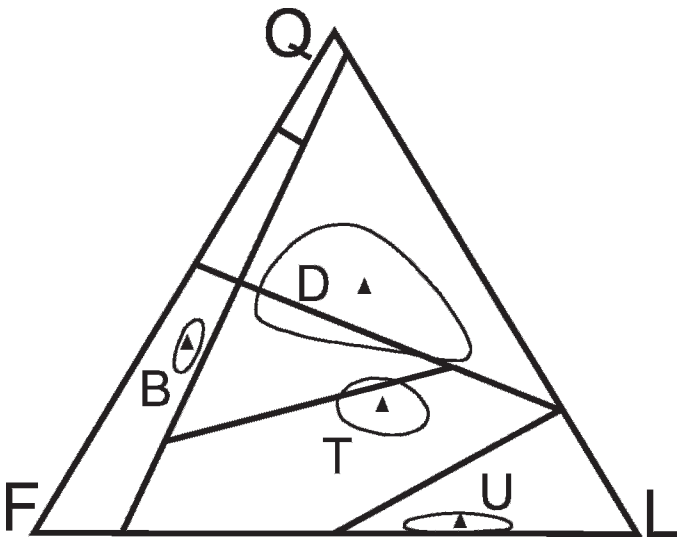


FIG. 8.—Ternary diagram showing Dickinson's (1985) provenance fields, with Weltje's (2002) geometric means and confidence regions (Fig. 6). Notice that, although the general form of geometric means and confidence regions (Weltje 2002) is similar to the general form of arithmetic means and hexagons based on 1 standard deviation (Ingersoll 1978), the values differ in detail (compare Figs. 6 and 7). Only arithmetic means of multiple specimens should be used with Dickinson's (1985) and related plots (e.g., Marsaglia and Ingersoll 1992) because these plots were created with this form of data.

available from the JSR Data Archive: http://www.sepm.org/archive/index.html.

## REFERENCES


AGUE, J.J., AND BRIMHALL, G.H., 1988, Magmatic arc asymmetry and distribution of anomalous plutonic belts in the batholiths of California: Effects of assimilation, crustal thickness, and depth of crystallization: Geological Society of America, Bulletin, v. 100, p. 912–927.

ATWATER, T., AND STOCK, J., 1998, Pacific–North America plate tectonics of the Neogene southwestern United States: an update: International Geology Review, v. 40, p. 375–402.

BATEMAN, P.C., 1992, Plutonism in the central part of the Sierra Nevada batholith, California: United States Geological Survey, Professional Paper 1483, 186 p.

BIRD, P., 1988, Formation of the Rocky Mountains, western United States: a continuum computer model: Science, v. 239, p. 1501–1507.

BURCHFIEL, B.C., COWAN, D.S., AND DAVIS, G.A., 1992, Tectonic overview of the Cordilleran orogen in the western United States, *in* Burchfiel, B.C., Lipman, P.W., and Zoback, M.L., eds., The Cordilleran Orogen: Conterminous U.S.: Geological Society of America, The Geology of North America, v. G-3, p. 407–480.

BUSBY-SPERA, C.J., 1988, Speculative tectonic model for the early Mesozoic arc of the southwest Cordilleran United States: Geology, v. 16, p. 1121–1125.

BUSBY-SPERA, C.J., AND SALEEBY, J., 1990, Intra-arc strike-slip fault exposed at batholithic levels in the southern Sierra Nevada, California: Geology, v. 18, p. 255–259.

CHASE, C.G., AND WALLACE, T.C., 1986, Uplift of the Sierra Nevada, California: Geology, v. 14, p. 730–733.

CHEN, J.H., AND MOORE, J.G., 1982, Uranium–lead isotopic ages from the Sierra Nevada batholith, California: Journal of Geophysical Research, v. 87, p. 4761–4784.

CHRISTENSEN, M.N., 1966, Late Cenozoic crustal movements in the Sierra Nevada of California: Geological Society of America, Bulletin, v. 77, p. 163–182.

CHRISTIANSEN, R.L., AND YEATS, R.S., 1992, Post-Laramide geology of the U.S. Cordilleran region, *in* Burchfiel, B.C., Lipman, P.W., and Zoback, M.L., eds., The Cordilleran Orogen: Conterminous U.S.: Geological Society of America, The Geology of North America, v. G-3, p. 261–403.

COLEMAN, D.S., AND GLAZNER, A.F., 1997, The Sierra Crest magmatic event: rapid formation of juvenile crust during the Late Cretaceous in California: International Geology Review, v. 39, p. 768–787.

CONEY, P.J., AND REYNOLDS, S.J., 1977, Cordilleran Benioff zones: Nature, v. 270, p. 403–406.

COWAN, D.S., AND BRUHN, R.L., 1992, Late Jurassic to early Late Cretaceous geology of the U.S. Cordillera, *in* Burchfiel, B.C., Lipman, P.W., and Zoback, M.L., eds., The Cordilleran Orogen: Conterminous U.S.: Geological Society of America, The Geology of North America, v. G-3, p. 169–203.

CROUGH, S.T., AND THOMPSON, G.A., 1977, Upper-mantle origin of the Sierra Nevada uplift: Geology, v. 5, p. 396–399.

DECELLES, P.G., 2004, Late Jurassic to Eocene evolution of the Cordilleran thrust belt and foreland basin system, western U.S.A.: American Journal of Science, v. 304, p. 105–168.

DICKINSON, W.R., 1985, Interpreting provenance relations from detrital modes of sandstones, *in* Zuffa, G.G., ed., Provenance of Arenites: Boston, D. Reidel, p. 333–361.

DICKINSON, W.R., 1997, Tectonic implications of Cenozoic volcanism in coastal California: Geological Society of America, Bulletin, v. 109, p. 936–954.

DICKINSON, W.R., 2002, The Basin and Range province as a composite extensional domain: International Geology Review, v. 44, p. 1–38.

DICKINSON, W.R., AND LAWTON, T.F., 2003, Sequential intercontinental suturing as the ultimate control for Pennsylvanian ancestral Rocky Mountains deformation: Geology, v. 31, p. 609–612.

DICKINSON, W.R., AND RICH, E.I., 1972, Petrologic intervals and petrofacies in the Great Valley sequence, Sacramento Valley, California: Geological Society of America, Bulletin, v. 83, p. 3007–3024.

DICKINSON, W.R., AND SNYDER, W.S., 1978, Plate tectonics of the Laramide orogeny, *in* Matthews, V, III, ed., Laramide folding associated with basement block faulting in the western United States: Geological Society of America, Memoir 151, p. 355–366.

DICKINSON, W.R., AND SNYDER, W.S., 1979, Geometry of triple junctions related to San Andreas transform: Journal of Geophysical Research, v. 84, p. 561–572.

DICKINSON, W.R., INGERSOLL, R.V., AND GRAHAM, S.A., 1979, Paleogene sediment dispersal and paleotectonics in northern California: Geological Society of America, Bulletin, v. 90, Part I, p. 897–898, Part II, p. 1458–1528.

DIXON, T.H., MILLER, M., FARINA, F., WANG, H., AND JOHNSON, D., 2000, Present-day motion of the Sierra Nevada block and some tectonic implications for the Basin and Range province, North American Cordillera: Tectonics, v. 19, p. 1–24.

DUMITRU, T.A., GANS, P.B., FOSTER, D.A., AND MILLER, E.L., 1991, Refrigeration of the western Cordilleran lithosphere during Laramide shallow-angle subduction: Geology, v. 19, p. 1145–1148.

EASTMOND, D.J., 2004. Composition of modern sand from the Sierra Nevada: constraints on actualistic petrofacies of continental-margin magmatic arcs [MS thesis]: University of California, Los Angeles, 103 p.

EASTMOND, D.J., AND INGERSOLL, R.V., 2003, Composition of modern sand from the Sierra Nevada: constraints on actualistic petrofacies of continental-margin magmatic arcs [abstract]: Geological Society of America, Abstracts with Programs, v. 35, no. 6, 465 p.

EVERNDEN, J.F., AND KISTLER, R.W., 1970, Chronology of emplacement of Mesozoic batholithic complexes in California and western Nevada: United States Geological Survey, Professional Paper 623, 42 p.

GODFREY, N.J., AND KLEMPERER, S.L., 1998, Ophiolitic basement to a forearc basin and Mesozoic implications for continental growth: the Coast Range/Great Valley ophiolite, California: Tectonics, v. 17, p. 558–570.

HAMILTON, W., 1978, Mesozoic tectonics of the western United States, *in* Howell, D.G., and McDougall, K.A., eds., Mesozoic Paleogeography of the Western United States: SEPM, Pacific Section, Pacific Coast Paleogeography Symposium 2, p. 33–70.

HOUSE, M.A., WERNICKE, B.P., AND FARLEY, K.A., 2001, Paleo-geomorphology of the Sierra Nevada, California, from (U−Th)/He ages in apatite: American Journal of Science, v. 301, p. 77–102.

HUBER, N.K., 1981, Amount and timing of late Cenozoic uplift and tilt of the central Sierra Nevada, California—evidence from the upper San Joaquin River basin: U.S. Geological Survey, Professional Paper 1197, 28 p.

ICHINOSE, G.A., SMITH, K.D., AND ANDERSON, J.G., 1998, Moment tensor solutions of the 1994 to 1996 Double Spring Flat, Nevada, earthquake sequence and implications for local tectonic models: Seismological Society of America, Bulletin, v. 88, p. 1363–1378.

INGERSOLL, R.V., 1978, Petrofacies and petrologic evolution of the Late Cretaceous fore-arc basin, northern and central California: Journal of Geology, v. 86, p. 335–352.

INGERSOLL, R.V., 1979, Evolution of the Late Cretaceous forearc basin, northern and central California: Geological Society of America, Bulletin, v. 90, part I, p. 813–826.

INGERSOLL, R.V., 1982, Triple-junction instability as cause for late Cenozoic extension and fragmentation of the western United States: Geology, v. 10, p. 621–624.

INGERSOLL, R.V., 1983, Petrofacies and provenance of late Mesozoic forearc basin, northern and central California: American Association of Petroleum Geologists, Bulletin, v. 67, p. 1125–1142.

INGERSOLL, R.V., 1990, Actualistic sandstone petrofacies: discriminating modern and ancient source rocks: Geology, v. 18, p. 733–736.

INGERSOLL, R.V., 1997, Phanerozoic tectonic evolution of central California and environs: International Geology Review, v. 39, p. 957–972.

INGERSOLL, R.V., 2000, Models for origin and emplacement of Jurassic ophiolites of northern California, *in* Dilek, Y., Moores, E.M., Elthon, D., and Nicolas, A., eds., Ophiolites and Oceanic Crust: New Insights from Field Studies and the Ocean Drilling Program: Geological Society of America, Special Paper 349, p. 395–402.

INGERSOLL, R.V., AND CAVAZZA, W., 1991, Reconstruction of Oligo-Miocene volcaniclastic dispersal patterns in north-central New Mexico using sandstone petrofacies, *in* Fisher, R.V., and Smith, G.A., eds., Sedimentation in Volcanic Settings: SEPM, Special Publication 45, p. 227–236.

INGERSOLL, R.V., AND EASTMOND, D.J., 2004, Composition of modern sand from the Sierra Nevada, California, USA: constraints on actualistic petrofacies of continental-margin magmatic arcs [abstract]: 32nd IGC Florence 2004—Scientific Sessions: abstracts (part 2), Florence, p. 1091.

Ingersoll, R.V., Bullard, T.F., Ford, R.L., Grimm, J.P., Pickle, J.D., and Sares, S.W., 1984, The effect of grain size on detrital modes: a test of the Gazzi–Dickinson point-counting method: Journal of Sedimentary Petrology, v. 54, p. 103–116.

Ingersoll, R.V., Kretchmer, A.G., and Valles, P.K., 1993, The effect of sampling scale on actualistic sandstone petrofacies: Sedimentology, v. 40, p. 937–953.

Jones, C.H., Farmer, G.L., and Unruh, J., 2004, Tectonics of Pliocene removal of lithosphere of the Sierra Nevada, California: Geological Society of America, Bulletin, v. 116, p. 1408–1422.

Keith, S.B., 1978, Paleosubduction geometries inferred from Cretaceous and Tertiary magmatic patterns in southwestern North America: Geology, v. 6, p. 516–521.

Keith, S.B., 1982, Paleoconvergence rates determined from $K_2O/SiO_2$ ratios in magmatic rocks and the application to Cretaceous and Tertiary tectonic patterns in southwestern North America: Geological Society of America, Bulletin, v. 93, p. 524–532.

Kistler, R.W., and Peterman, Z.E., 1973, Variations in Sr, Rb, K, Na, and Initial $Sr^{87}/Sr^{86}$ in Mesozoic granitic rocks and intruded wall rocks in central California: Geological Society of America, Bulletin, v. 84, p. 3489–3512.

Koch, G.S., Jr., and Link, R.F., 1971. Statistical Analysis of Geological Data, Volume II: New York, John Wiley & Sons, 438 p.

Kretchmer, A.G., 1987. Petrology and provenance of modern sands from the Cascade Range forearc and Canadian Rocky Mountain forearc [M.S. thesis]: Los Angeles, University of California, 216 p.

Lee, J., Spencer, J., and Owen, L., 2001, Holocene slip rates along the Owens Valley fault, California: implications for the recent evolution of the eastern California shear zone: Geology, v. 29, p. 819–822.

Leeder, M.R., 1995, Continental rifts and proto-oceanic rift troughs, *in* Busby, C.J., and Ingersoll, R.V., eds., Tectonics of Sedimentary Basins: Malden, Massachusetts, Blackwell Science, p. 119–148.

Leeder, M.R., and Gawthorpe, R.L., 1987, Sedimentary models for extensional tilt-block/half-graben basins, *in* Coward, M.P., Dewey, J.F., and Hancock, P.L., eds., Continental Extensional Tectonics: Geological Society of London, Special Publication 28, p. 139–152.

Linn, A.M., DePaolo, D.J., and Ingersoll, R.V., 1992, Nd–Sr isotopic, geochemical, and petrographic stratigraphy and paleotectonic analysis: Mesozoic Great Valley forearc sedimentary rocks of California: Geological Society of America, Bulletin, v. 104, p. 1264–1279.

Liu, M., and Shen, Y., 1998, Sierra Nevada uplift: A ductile link to mantle upwelling under the Basin and Range province: Geology, v. 26, p. 299–302.

Loomis, D.P., and Burbank, D.W., 1988, The stratigraphic evolution of the El Paso basin, southern California: Implications for the Miocene development of the Garlock fault and uplift of the Sierra Nevada: Geological Society of America, Bulletin, v. 100, p. 12–28.

Marsaglia, K.M., 1991, Provenance of sands and sandstones from a rifted continental arc, Gulf of California, Mexico, *in* Fisher, R.V., and Smith, G.A., eds., Sedimentation in Volcanic Settings: SEPM, Special Publication 45, p. 237–248.

Marsaglia, K.M., and Ingersoll, R.V., 1992, Compositional trends in arc-related, deep- marine sand and sandstone: A reassessment of magmatic-arc provenance: Geological Society of America, Bulletin, v. 104, p. 1637–1649.

Marsaglia, K.M., Torrez, X.V., Padilla, I., and Rimkus, K.C., 1995, Provenance of Pleistocene and Pliocene sand and sandstone, ODP Leg 141, Chile margin: Proceedings of the Ocean Drilling Program, Scientific Results, v. 141, p. 133–151.

Miller, E.L., Miller, M.M., Stevens, C.H., Wright, J.E., and Madrid, R., 1992, Late Paleozoic paleogeographic and tectonic evolution of the western U.S. Cordillera, *in* Burchfiel, B.C., Lipman, P.W., and Zoback, M.L., eds., The Cordilleran Orogen: Conterminous U.S.: Geological Society of America, The Geology of North America, v. G-3, p. 57–106.

Mulch, A., Graham, S.A., and Chamberlain, C.P., 2006, Hydrogen isotopes in Eocene River gravels and paleoelevation of the Sierra Nevada: Science, v. 313, p. 87–89.

Poole, F.G., Stewart, J.H., Palmer, A.R., Sandberg, C.A., Madrid, R.J., Ross, R.J., Jr., Hintze, L.F., Miller, M.M., and Wrucke, C.T., 1992, Latest Precambrian to latest Devonian time; development of a continental margin, *in* Burchfiel, B.C., Lipman, P.W., and Zoback, M.L., eds., The Cordilleran Orogen: Conterminous U.S.: Geological Society of America, The Geology of North America, v. G-3, p. 9–56.

Ramelli, A.R., Bell, J.W., dePolo, C.M., and Yount, J.C., 1999, Large-magnitude, late Holocene earthquakes on the Genoa fault, west-central Nevada and eastern California: Seismological Society of America, Bulletin, v. 89, p. 1458–1472.

Ruppert, S., Fliedner, M.M., and Zandt, G., 1998, Thin crust and active upper mantle beneath the southern Sierra Nevada in the western United States: Tectonophysics, v. 286, p. 237–252.

Ryall, A.S., and Van Wormer, J.D., 1980, Estimation of maximum magnitude and recommended seismic zone changes in the western Great Basin: Seismological Society of America, Bulletin, v. 70, p. 1573–1581.

Saleeby, J.B., and Busby-Spera, C., 1992, Early Mesozoic tectonic evolution of the western U.S. Cordillera, *in* Burchfiel, B.C., Lipman, P.W., and Zoback, M.L., eds., The Cordilleran Orogen: Conterminous U.S.: Geological Society of America, The Geology of North America, v. G-3, p. 107–168.

Saleeby, J.B., Sams, D.B., and Kistler, R.W., 1987, U/Pb zircon, strontium, and oxygen isotopic and geochronological study of the southernmost Sierra Nevada batholith, California: Journal of Geophysical Research, v. 92, p. 10,443–10,466.

Saleeby, J.B., Ducea, M., and Clemens-Knott, K., 2003, Production and loss of high-density batholithic root, southern Sierra Nevada, California Tectonics, v. 22, no. 6, p. 3-1–3-24.

Schweickert, R.A., 1976, Shallow-Level Plutonic Complexes in the Eastern Sierra Nevada, California, and Their Tectonic Implications: Geological Society of America, Special Paper 176, 58 p.

Schweickert, R.A., 1981, Tectonic evolution of the Sierra Nevada range, *in* Ernst, W.G., ed., Geotectonic Development of California [Rubey Volume I]: Englewood Cliffs, New Jersey, Prentice-Hall, p. 87–131.

Schweickert, R.A., and Cowan, D.S., 1975, Early Mesozoic tectonic evolution of the western Sierra Nevada, California: Geological Society of America, Bulletin, v. 86, p. 1329–1336.

Small, E.E., and Anderson, R.S., 1995, Geomorphically driven late Cenozoic rock uplift in the Sierra Nevada, California: Science, v. 270, p. 277–280.

Speed, R.C., 1979, Collided Paleozoic microplate in the western United States: Journal of Geology, v. 87, p. 279–292.

Speed, R.C., and Sleep, N.H., 1982, Antler orogeny and foreland basin: A model: Geological Society of America, Bulletin, v. 93, p. 815–828.

SPSS, 2000, Systat 10: SPSS, Inc., Chicago, variable pagination.

Stern, T.W., Bateman, P.C., Morgan, B.A., Newell, M.F., and Peck, D.L., 1981, Isotopic U–Pb ages of zircon from the granitoids of the central Sierra Nevada, California: United States Geological Survey, Professional Paper 1185, 17 p.

Tabachnick, B.G., and Fidell, L.S., 2001. Using Multivariate Statistics: Boston, Allyn and Bacon, 966 p.

Tikoff, B., and de Saint Blanquat, M., 1997, Transpressional shearing and strike-slip partitioning in the Late Cretaceous Sierra Nevada magmatic arc, California: Tectonics, v. 16, p. 442–459.

Tobisch, O.T., Saleeby, J.B., Renne, P.R., McNultry, B., and Tong, W., 1995, Variations in deformation fields during development of a large volume magmatic arc, central Sierra Nevada, California: Geological Society of America, Bulletin, v. 107, p. 148–166.

Unruh, J.R., 1991, The uplift of the Sierra Nevada and implications for late Cenozoic epeirogeny in the western Cordillera: Geological Society of America, Bulletin, v. 103, p. 1395–1404.

Van Wormer, J.D., and Ryall, A.S., 1980, Sierra Nevada–Great Basin boundary zone: earthquake hazard related to structure, active tectonic processes, and anomalous patterns of earthquake occurrence: Seismological Society of America, Bulletin, v. 70, p. 1557–1572.

Wakabayashi, J., and Sawyer, T.L., 2001, Stream incision, tectonics, uplift, and evolution of topography of the Sierra Nevada, California: Journal of Geology, v. 109, p. 539–562.

Ward, P.L., 1991, On plate tectonics and the geologic evolution of southwestern North America: Journal of Geophysical Research, v. 96, p. 12,479–12,496.

Weissmann, G.S., Mount, J.F., and Fogg, G.E., 2002, Glacially driven cycles in accumulation space and sequence stratigraphy of a stream-dominated alluvial fan, San Joaquin Valley, California, U.S.A.: Journal of Sedimentary Research, v. 72, p. 240–251.

Weltje, G.J., 2002, Quantitative analysis of detrital modes: statistically rigorous confidence regions in ternary diagrams and their use in sedimentary petrology: Earth-Science Reviews, v. 57, p. 211–253.

Weltje, G.J., 2004, A quantitative approach to capturing the compositional variability of modern sands: Sedimentary Geology, v. 171, p. 59–77.

Wernicke, B.P., Clayton, R., Ducea, M., Jones, C.H., Park, S., Ruppert, S., Saleeby, J., Snow, J.K., Squires, L., Fliedner, M., Jiracek, G., Keller, R., Klemperer, S., Luetgert, J., Malin, P., Miller, K., Mooney, W., Oliver, H., and Phinney, R., 1996, Origin of high mountains in the continents: the southern Sierra Nevada: Science, v. 271, p. 190–193.

Wesnousky, S.G., and Jones, C.H., 1994, Oblique slip, slip partitioning, spatial and temporal changes in the regional stress field, and the relative strength of active faults in the Basin and Range, western United States: Geology, v. 22, p. 1031–1034.

Zandt, G., Gilbert, H., Owens, T.J., Ducea, M., Saleeby, J., and Jones, C.H., 2004, Active foundering of a continental arc root beneath the southern Sierra Nevada in California: Nature, v. 431, p. 41–46.

Zoback, M.L., 1989, State of stress and modern deformation of the northern Basin and Range province: Journal of Geophysical Research, v. 94, p. 7105–7128.

Zuffa, G.G., 1985, Optical analyses of arenites: influence of methodology on compositional results, *in* Zuffa, G.G., ed., Provenance of Arenites: Dordrecht, The Netherlands, D. Reidel Publishing Co., p. 165–189.

Received 7 August 2006; accepted 7 March 2007.